

Diffraction effects upon finite-frequency travel times: a simple 2-D example

Jun Tong, F. A. Dahlen, Guust Nolet and Henk Marquering

Department of Geosciences, Princeton University, Princeton, New Jersey

Abstract. The widespread availability of broad-band digital seismic data makes it possible to measure travel-time anomalies by cross-correlation with spherical-earth synthetic seismograms. Finite-frequency diffraction effects render such measurements sensitive to wave-speed perturbations off of the infinite-frequency geometrical ray path. We show, by consideration of a simple 2-D example, that the Born approximation provides an excellent description of these off-path sensitivity effects, in the absence of caustics and for travel-time shifts that are small compared to the wave period. Remarkably, an isolated low-velocity anomaly may produce fringing fast travel-time anomalies, as measured by cross-correlation.

Introduction

It is well known that geometrical ray theory describes wave propagation correctly in the limit of high frequencies. If the frequencies are not high enough, the usual understanding is that ray theory is no longer suited for amplitude calculations, but that travel times can still be modeled correctly [Witte, Roth and Müller, 1996]. However, we show in this study that travel times measured by cross-correlation of broad-band pulses are significantly affected by finite-frequency diffraction effects. When the scale length of the structure is comparable to the wave length, ray theory is no longer valid, and more sophisticated inversion schemes have to be used.

Cross-correlation travel time

A number of authors have recently studied the sensitivity of seismic waves using various approaches [Woodward, 1992; Li & Tanimoto, 1993; Vasco & Majer, 1993; Marquering & Snieder, 1995; Snieder & Lomax, 1996; Marquering, Nolet & Dahlen, 1998]. Here, we combine the Born approximation with a cross-correlation technique [VanDecar & Crosson, 1990; Woodward & Masters, 1991] to calculate the sensitivity kernel of a finite-frequency travel-time measurement in 2-D. In the frequency domain, the 2-D scalar wave equation is:

$$(\nabla^2 + k^2)\tilde{u} = -\tilde{f}(\omega)\delta(\mathbf{r} - \mathbf{s}), \quad (1)$$

where the tilde represents the Fourier transform. Our sign convention is that $e^{i\omega t}$ appears in the Fourier integral in transforming from time t to frequency ω . The quantity \tilde{u} is the displacement, \tilde{f} encapsulates the frequency dependence of the point source, and k is the

wave number defined by $k = \omega/c$, where c is the wave speed. The vector \mathbf{r} specifies the position of the receiver, and \mathbf{s} is the source location. Born theory only considers a single scatterer and assumes the following linearized relation: $u = u_0 + u_1$, where u_0 is the background homogeneous-medium seismogram, and u is the inhomogeneous-medium seismogram which differs from u_0 by the first-order perturbation u_1 . The Green function in a weakly inhomogeneous medium is also linearized: $G = G_0 + G_1$, where G_0 is the Green function for the homogeneous medium and G_1 is the first-order perturbation. In the frequency domain, \tilde{G}_0 is a Hankel function: $\tilde{G}_0(R, \omega) = (i/4)H_0^{(1)}(kR)$, where $R = |\mathbf{r} - \mathbf{s}|$ is the distance between the source and the receiver. In the far field, we use the following approximation:

$$\tilde{G}_0(R, \omega) \approx (i/4)\sqrt{2/(\pi k R)} e^{i(kR - \pi/4)}. \quad (2)$$

The first-order perturbation of the Green function is given by

$$\tilde{G}_1(R, \omega) = \iint_A \tilde{G}_0(R_1, \omega) \delta k^2 \tilde{G}_0(R_2, \omega) dx, \quad (3)$$

where the integration is carried over all of space A . The quantity $R_1 = |\mathbf{s} - \mathbf{x}|$ is the distance between the source and the scatterer, and $R_2 = |\mathbf{x} - \mathbf{r}|$ is the distance between the scatterer and the receiver. The squared wave number perturbation δk^2 in (3) is related to the perturbation δc in the wave speed by $\delta k^2 = -2(\omega/c)^2(\delta c/c)$. The relations between the Green functions and the seismograms are

$$\tilde{u}_0(R, \omega) = \tilde{G}_0(R, \omega)\tilde{f}(\omega), \quad (4)$$

$$\tilde{u}_1(R, \omega) = \tilde{G}_1(R, \omega)\tilde{f}(\omega). \quad (5)$$

If we cross-correlate the homogeneous-medium seismogram with the perturbed seismogram, the cross-correlation function is

$$C(\tau) = \int_{-\infty}^{\infty} u_0(t - \tau)[u_0(t) + u_1(t)]dt. \quad (6)$$

We define the unperturbed cross-correlation function $C_0(\tau) = \int_{-\infty}^{\infty} u_0(t - \tau)u_0(t)dt$ and perturbed function $C_1(\tau) = \int_{-\infty}^{\infty} u_0(t - \tau)u_1(t)dt$. For small shifts, which we shall denote by $\delta\tau$ rather than τ , we expand (6) in a Taylor series about zero, keeping terms of second order in the perturbation δc :

$$C(\delta\tau) = C_0(0) + \delta\tau\partial_\tau C_0(0) + \frac{1}{2}\delta\tau^2\partial_{\tau\tau} C_0(0) + C_1(0) + \delta\tau\partial_\tau C_1(0). \quad (7)$$

Copyright 1998 by the American Geophysical Union.

Paper number 98GL01291.
0094-8534/98/98GL-01291\$05.00

In applications, the time shift $\delta\tau$ is determined by finding the maximum of the cross-correlation function:

$$\partial_{\delta\tau} C(\delta\tau) = 0. \quad (8)$$

Bearing in mind that the unperturbed cross-correlation has its maximum at zero, $\partial_{\tau} C_0(0) = 0$, we obtain

$$\delta\tau = -\frac{\partial_{\tau} C_1(0)}{\partial_{\tau} C_0(0)} = \frac{\int_{-\infty}^{\infty} \dot{u}_0 u_1 dt}{\int_{-\infty}^{\infty} \ddot{u}_0 u_0 dt}, \quad (9)$$

where the dot denotes differentiation with respect to time. Parseval's theorem can be used to convert the numerator and denominator in (9) to the frequency domain:

$$\delta\tau = -\frac{Re \int_0^{\infty} i\omega \tilde{u}_0^* \tilde{u}_1 d\omega}{\int_0^{\infty} \omega^2 |\tilde{u}_0|^2 d\omega}, \quad (10)$$

where the asterisk denotes complex conjugation. Upon inserting (2)–(5) into (10) and interchanging the order of integration, so that we integrate first over frequency ω , we can write the time shift in the form

$$\delta\tau = \iint_A K(\mathbf{x}) \delta c(\mathbf{x}) d\mathbf{x}. \quad (11)$$

The quantity $K(\mathbf{x})$ is a two-dimensional Fréchet travel time kernel given explicitly by

$$K(\mathbf{x}) = -\frac{\int_0^{\infty} \sqrt{\omega^3} |\tilde{f}(\omega)|^2 \cos\left[\frac{\omega}{c}(R_1 + R_2 - R) - \frac{\pi}{4}\right] d\omega}{\sqrt{2\pi c^5} R_1 R_2 / R \int_0^{\infty} \omega |\tilde{f}(\omega)|^2 d\omega}. \quad (12)$$

The time shift depends upon the frequency content of the cross-correlated pulse through the power spectrum $|\tilde{f}(\omega)|^2$. In the limit $\omega \rightarrow \infty$, the spatial oscillations of the wave-speed perturbation $\delta c(\mathbf{x})$ are much smoother than those of the kernel $K(\mathbf{x})$; the method of stationary phase can then be used to evaluate the cross-path integral in (11), with the result

$$\delta\tau \sim -c^{-2} \int_0^R \delta c(x) ds, \quad (13)$$

where ds is measured along the straight ray between \mathbf{s} and \mathbf{r} . This is the ray-theoretical travel time shift in the Fermat or straight-ray approximation, as expected.

Finite-difference calculation

We test the above expectation by comparison with two-dimensional finite-difference calculations. The ex-

act response is obtained by solving the wave equation numerically in the time domain:

$$\nabla^2 u - (1/c^2) \partial^2 u / \partial t^2 = -f(t) \delta(\mathbf{r} - \mathbf{s}), \quad (14)$$

$$u(\mathbf{r}, 0) = \partial u(\mathbf{r}, 0) / \partial t = 0. \quad (15)$$

An absorbing boundary condition is used upon the four outer boundaries to suppress unwanted reflections (Reynolds, 1978). In this study, we use a broad-band point-source time function,

$$f(t) = (1/10)t^2 e^{-(\pi t/45)^2} \cos[(\pi t/15) - (\pi/2)], \quad (16)$$

with a dominant period of 30 seconds. Since the background velocity is 8 km/s, the average wavelength, λ , is 240 km. We calculate a seismogram in a heterogeneous medium, shown as the solid curve in Figure 1, and a seismogram at the same receiver in the homogeneous background medium, shown as the dashed line (see below for a description of the velocity perturbation). For receivers between grid points, we use two-dimensional bilinear interpolation to compute the displacement seismograms. To measure the travel times, we cross-correlate the two seismograms and determine the position of the maximum by parabolic curve-fitting. The acausal blip at the beginning of the pulse is an artifact due to grid dispersion. This should not influence our travel time measurement significantly because the grid dispersion effect on the perturbed and unperturbed seismograms at a given receiver is approximately the same. The parameters for our experiment are chosen such that they are roughly representative for delay-time measurements using long-period sensors. Our results are therefore relevant for tomographic interpretations of teleseismic S waves [e.g. Woodward & Masters, 1991].

Ray tracing and Fermat travel times

We also compare the measured travel time with ray-theoretical ($\omega \rightarrow \infty$) predictions. The two-dimensional ray-tracing equations are:

$$dp_x/ds = \partial\gamma/\partial x, \quad dp_y/ds = \partial\gamma/\partial y, \quad (17)$$

$$\gamma dx/ds = p_x, \quad \gamma dy/ds = p_y. \quad (18)$$

where s is the arc length measured along the refracted ray path, $\gamma = c^{-1}$ is the slowness distribution, (x, y) is the position vector, and $(p_x, p_y) = \omega(k_x, k_y)$ is the wave slowness vector. The initial conditions are

$$x(0) = 0, \quad y(0) = 0, \quad (19)$$

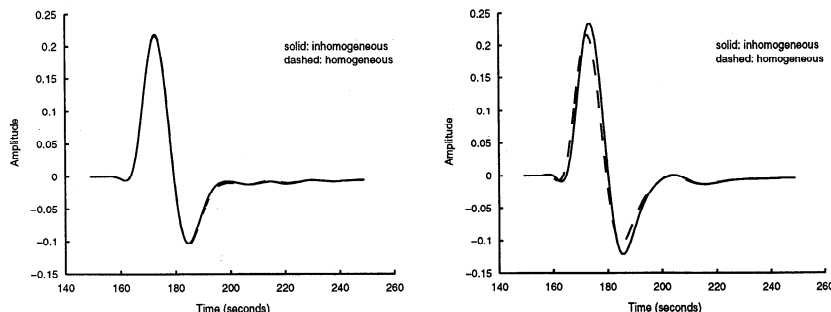


Figure 1. (Left) Seismograms at receiver 5 (azimuth 15°) computed using the finite-difference code. See Figure 2 for an explanation of the velocity anomaly $\delta c(\mathbf{x})$ and the source-receiver configuration. (Right) Same except that the calculations are carried out at receiver 15 (azimuth 45°) where the maximum travel-time delay occurs.

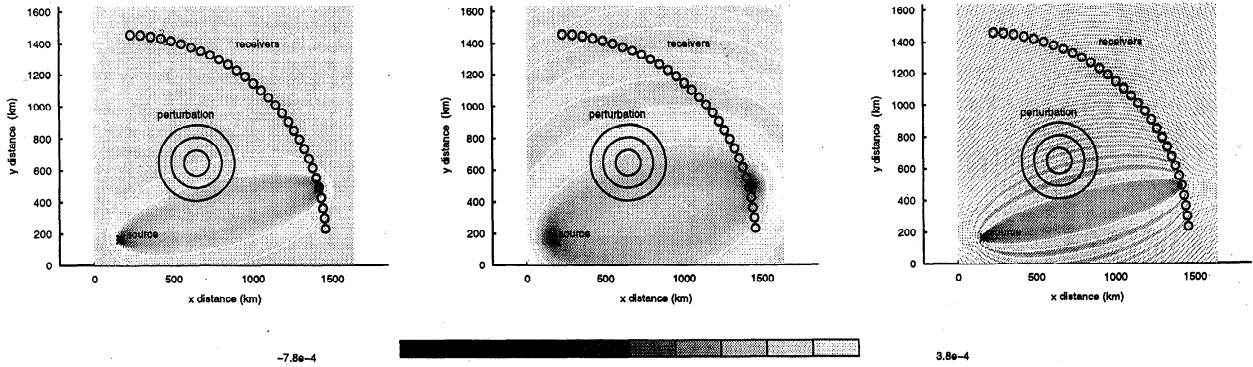


Figure 2. (Left) Model configuration and the broad-band ($a/\lambda = 0 - 36$) sensitivity kernel for receiver 5. The source is in the left corner at the bottom. Receivers are situated at the small circles. The concentric circles in the middle are contours of the velocity anomaly $\delta c(\mathbf{x})$. Shading shows the kernel $K(\mathbf{x})$; zero values are the white contours. The sign of $K(\mathbf{x})$ is negative in the central dark ellipse. (Middle) Same except that the kernel is filtered by a low-pass filter ($a/\lambda = 0 - 1$). (Right) Same except that the kernel is filtered by a high-frequency narrow-band filter ($a/\lambda = 7 - 8$).

$$p_x(0) = p_{x_0}, \quad p_y(0) = p_{y_0}. \quad (20)$$

The initial takeoff angles change from 0° to 90° , measured counter-clockwise. We solve equations (17)–(20) using a fourth-order Runge-Kutta algorithm. The velocity between grid points is calculated by means of a two-dimensional cubic spline interpolation. The two-point travel-time anomaly at a particular receiver is found using a simple bisection-based shooting method; specifically, we compute

$$\delta\tau = \int_{\Gamma}^S \frac{ds}{c + \delta c} - \int_0^R \frac{ds}{c}, \quad (21)$$

where the first and second integrals are evaluated along the curved and straight rays, respectively. The time (13) based upon the Fermat or straight-ray approximation is also computed. Provided that the true ray has not passed through a caustic, we expect $\delta\tau_{\text{Fermat}}$ to be always *greater* than $\delta\tau_{\text{true ray}}$, in accordance with Fermat’s principle of least time.

Comparison

We consider the travel-time delay produced by a single bell-shaped low-velocity anomaly, of the form $\delta c = -0.04 c[1 + \cos(2\pi r/a)]$, embedded in a homoge-

neous background field (see Figure 2). The cosine shape has a smooth derivative on the boundary, to avoid a sudden bending of the ray. The source is located at the left bottom corner of the field; the receivers are all the same distance away from the source (see Figure 2). We will use this configuration in all of our studies.

Figure 3 compares the four travel-time anomaly measurements. Since the broad-band pulse consists of different frequency components with different wave lengths λ , the ratio a/λ varies from 0 to 37. The travel time in the background model is the horizontal line at 161.69 seconds. The curves show that the Born approximation (11) yields an excellent approximation to the measured cross-correlation travel time. However, diffraction effects lead to significant departures from ray theory. The first-order Fermat travel time (13) is always later than the true ray-theoretical time (21) measured along the refracted ray, as expected. An unexpected result is that, in this low-velocity anomaly model, the arrival times determined by cross-correlation are even earlier than in the background model in the diffraction “sidebands” at the 15° and 75° receiver azimuths.

In order to understand the mechanism of this phenomenon, we calculate the travel-time sensitivity kernel, $K(\mathbf{x})$, at receiver azimuth 15° in the broad-band frequency range (see Figure 2). The dark ellipse is the first negative Fresnel zone of the kernel. In the outer

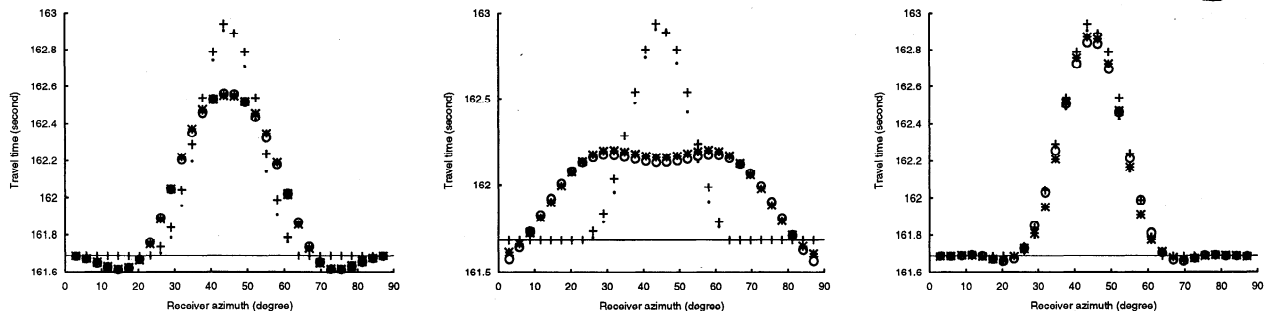


Figure 3. (Left) Four types of broad-band ($a/\lambda = 0 - 36$) travel times plotted versus the receiver azimuth, showing the diffraction effect. The open circles \circ are the theoretical cross-correlation travel times based upon the Born approximation (11) – (12). The asterisks $*$ are the cross-correlation travel times measured using the finite-difference seismograms. The ray tracing results (21) are shown as the dots \cdot and the first-order Fermat results (13) as the plus signs $+$. (Middle) Same except that seismograms have been low-pass filtered, so that $a/\lambda = 0 - 1$. (Right) Same except that seismograms have been high-pass filtered, so that $a/\lambda = 7 - 8$.

fringing Fresnel zone, $K(x)$ is positive. The two white elliptical curves are zero contours. The kernel has a small local maximum in the bottom of the dark minimum, right along the geometrical ray path, and a global maximum in the second Fresnel zone. The character of the broad-band kernel is not in accordance with ray theory, which predicts that the travel-time anomaly $\delta\tau$ should be sensitive to the wave speed perturbation $\delta c(x)$ only right along the ray. The amplitudes of the oscillating zones decrease as the distance increases from the ray path and the outer zones tend to cancel as result of destructive interference in the broad-band kernel (Figure 2). We can see from equation (11) that only the negative zone senses the anomaly in the expected intuitive sense — a slow perturbation gives a positive delay time. The fringing positive zone senses the anomaly as a fast contribution to the anomaly $\delta\tau$. The total anomaly (11) is the summation of all the contributions. Thus, at 15° and 75° , it gives an even earlier arrival than in the background model. What we see in figure 3-a is the effect of diffraction on cross-correlation travel times. All observed waves are of finite frequency and are sensitive to the perturbations $\delta c(x)$ off the geometrical ray. Diffraction causes a blunting of the travel-time anomaly due to wavefront healing effects [Gudmundsson, 1996]. While an early arrival might at first sight seem to violate the principle of causality, this is not the case: what happens is that within the time window for cross-correlation some of the energy is shifted towards earlier arrival times, so we stay on sound physical ground.

In order to study the low-frequency situation, we filter the seismograms with a low-pass filter. Changing the frequency component in the seismogram is equivalent to changing the dominant frequency in the source, and thus the ratio a/λ . In figure 3-b, a/λ is in the range 0 – 1. An even larger difference between the cross-correlation travel time and the ray-theoretical travel time is now evident. An interesting phenomenon is that the travel times at 15° and 75° are now above the background line. This indicates that waves with different frequencies sense the anomaly with different widths. Finite-frequency waves tend to smooth things over about one wave length [Lomax & Snieder, 1996]. Figure 2-b is the plot of the kernel in this frequency range. Here, we see more zones because they are not cancelled by the zones from other frequency ranges. However, the first zone is always constructive because all the first zones in different frequency ranges are negative. As expected, at higher frequencies, the agreement with ray theory is excellent (see Figure 3-c). This result is obtained by filtering the seismograms with a narrow band-pass filter, so that the ratio a/λ is 7 – 8. The corresponding high-frequency kernel in this case is shown in Figure 2-c.

Conclusions and Discussion

The results of this simple study show that, in the absence of triplications, the Born approximation (11) can

be used to predict the effect of off-path velocity anomalies $\delta c(x)$ upon the travel-time $\delta\tau$ measured by cross-correlation of broad-band pulses. However, diffraction effects lead to significant departures from ray theory. The Fermat travel time (13) is always later than the true ray-theoretical time (21) measured along the refracted ray, as expected. An unexpected result is the apparently acausal character of the cross-correlation travel times measured on paths that graze an isolated low-velocity anomaly.

Acknowledgments. We thank Henk Keers for supplying the ray-tracing code used in this calculation and Sergei Lebedev for numerous discussions during the final stages of this research. This research was supported by NSF grant EAR-9218926.

References

- Gudmundsson, O., On the effect of diffraction on travel-time measurements, *Geophys. J. Int.* **124**, 304-314, 1996.
- Li, X.-D., and T. Tanimoto, Waveforms of long-period body waves in a slightly aspherical Earth model, *Geophys. J. Int.*, **112**, 92-102, 1993.
- Lomax, A., and Snieder, R., Estimation of finite-frequency waveforms through wavelength-dependent averaging of velocity, *Geophys. J. Int.*, **126**, 369-381, 1996.
- Luo, Y., and G. T. Schuster, Wave equation inversion of skeletalized geophysical data, *Geophys. J. Int.*, **105**, 289-294, 1991.
- Marquering, H., G. Nolet and F. A. Dahlen, 3-D waveform sensitivity kernels, *Geophys. J. Int.* **132**, 521-534, 1998.
- Marquering, H., and R. Snieder, Surface-wave mode coupling for efficient forward modelling and inversion of body-wave phases, *Geophys. J. Int.*, **120**, 186-208, 1995.
- Reynolds, Albert C., Boundary conditions for the numerical solution of wave propagation problems, *Geophysics*, **43**, 1099-1110, 1978.
- Snieder, R., and A. Lomax, Wavefield smoothing and the effect of rough velocity perturbations on arrival times and amplitudes, *Geophys. J. Int.*, **125**, 796-812, 1996.
- VanDecar, J. C., and R. S. Crosson, Determination of teleseismic relative phase arrival times using multi-channel cross-correlation and least squares, *Bull. seism. Soc. Am.*, **80**, 150-159, 1990.
- Vasco, D. W., and E. L. Majer, Wavepath traveltime tomography, *Geophys. J. Int.*, **115**, 1055-1069, 1993.
- Witte, O., Roth, M. and Müller, G., Ray tracing in random medium, *Geophys. J. Int.* **124**, 159-169, 1996.
- Woodward, M.J., Wave-equation tomography, *Geophysics*, **57**, 15-26, 1992.
- Woodward, R. L., and G. Masters, Global upper mantle structure from long-period differential times, *J. Geophys. Res.*, **96**, 6351-6377, 1991.

J. Tong, F.A.Dahlen, G.Nolet, H.Marquering, Department of Geosciences, Princeton University, Princeton, New Jersey 08544

(Received January 13, 1998; revised April 3, 1998; accepted April 9, 1998.)